Energetic, Electronic, and Thermal Effects on Structural Properties of Ag−Au Nanoalloys

Fuyi Chen[†,‡] and Roy L. Johnston[†,*]

[†]School of Chemistry, University of Birmingham, Edgbaston, Birmingham B15 2TT, U.K., and [‡]State Key Laboratory of Solidification Processing, Northwestern Polytechnic University, Xian 710072, P. R. China

ARTICLE

ABSTRACT Using a genetic algorithm global optimization approach combined with density functional theory calculations, a search has been made for the lowest energies of $(AgAu)_m$ nanoalloys with 20−150 atoms (diameters of 1.0–2.0 nm). A total of 31 decahedra, 35 icosahedra, and 2 close-packed motifs are identified in two icosahedral windows and one Marks-decahedral window. These structural motifs have twinned, capped, defective, and distorted atomic packing compared to classical clusters, such as the icosahedron. The magic numbers, atomic ordering, electronic structure, and melting behavior are further studied, and a new poly-nanocrystalline decahedral motif, $Ag_{44}Au_{44}$, is found to have high structural, electronic, and thermal stability. Our results show that alloying can lead to a remarkable stabilization of local order and provide a comprehensive model for the structures and properties of Ag−Au nanoalloys.

KEYWORDS: global optimization · nanoalloy · size · structure · electronic and thermal stability

Metal clusters containing from two to several hundred atoms have size-dependent properties analogous to those of atomic nuclei, such as shell structure and "magic numbers".[1] These clusters are interesting examples of the size evolution from atomic to metallic behavior between atomic and solid-state physics. Global optimization[2] of metal clusters can give insight into how different properties evolve with size, since it can predict the ground-state geometry for a given composition in cases where no direct experiment is possible. Much recent interest in finding the global minima of cluster structures is focused on bimetallic clusters or "nanoalloys".[3] Nanoalloys offer the opportunity to tailor the structures and properties of clusters through the choice of atom type and composition in addition to size. For example, the surface plasmon resonance (SPR) energy of Ag−Au nanoalloys can be tuned by varying size and composition independently.[4] Mixed Ag−Au nanoalloys exhibit dipole SPR modes,[5] and core–shell segregated nanoalloys exhibit quadrupole SPR modes.[6]

Nanoalloys also offer considerable additional challenges for global optimization compared to pure metal clusters. There are many more minima on the potential energy surface due to the presence of inequivalent permutational isomers ("homotops"),[7] and the composition provides an additional variable that adds to the complexity of the structural behavior. In addition, there may be disordered clusters.[8] To overcome such difficulties, methods such as genetic algorithms (GA)[9,10] and basin-hopping algorithms[11,12] have been used for the global optimization of cluster geometries, such as Lennard-Jones,[10–16] metal,[17–30] molecular,[31] semiconductor,[32,33] alloy,[34–37] and compound[38–41] clusters.

Lennard-Jones clusters with $n = 20$–150 have been intensively studied using GA[10,13,14] and basin-hopping techniques.[11,12,16] The dominant structural motifs are icosahedral clusters for $n < 150$, and there are only eight non-icosahedral global minima. There are two face-centered cubic (fcc)-based motifs at $n = 38$ (truncated octahedron) and 98 (Leary tetrahedron[15]) and six decahedral clusters at $n =$ 75–77 and 102–104.

Gold clusters are probably the most widely investigated noble metal clusters. Most of the lowest-energy structures of Au_n clusters obtained from GA optimizations[17–19] using the Gupta potential (see Table 1) are disordered or low-symmetry structures,even for magic sizes. For example, Au_{55} and Au_{75} are disordered structures, which have been further confirmed by density functional theory (DFT) relaxations.[17,18] However, the stable structures for gold clusters obtained from the basin-hopping method using Sutton−Chen potentials[20] in this size range are the

*Address correspondence to r.l.johnston@bham.ac.uk.

Received for review September 11, 2007 and accepted November 29, 2007.

Published online December 22, 2007.
10.1021/nn700226y CCC: $40.75

TABLE 1. Gupta Potential Parameters

	parameters				
	A/eV	r_0/Å	ξ/eV	*p*	*q*
Au−Au	0.2096	2.8850	1.8153	10.139	4.033
Ag−Au	0.1488	2.8885	1.4874	10.494	3.607
Ag−Ag	0.1031	2.8921	1.1895	10.850	3.180

truncated octahedron and Marks decahedron. Typically, the Au_{13}[21,22] and Au_{147}[21,23] clusters are magic icosahedra. Au_{55} and Au_{75} are disordered structures,[22] and Au_{38},[22] Au_{79},[22,23] and Au_{140}[23] clusters are (truncated) octahedra. Au_{101},[23] Au_{116},[23] and Au_{146}[23,24] are Marks decahedra. In addition to these theoretical investigations, a Marks decahedral motif has recently been confirmed by X-ray powder diffraction analysis to form the core of a passivated Au_{102}[42] nanocluster.

For silver clusters in the range from Ag_{13} to Ag_{80},[22] as predicted from Sutton−Chen potentials, there are 30 icosahedral global minima, with Ag_{13} and Ag_{55} icosahedra as the most stable structures. There are 29 decahedral global minima, while the others present close-packed morphologies including hexagonal close packing, face-centered cubic, and a mixture of stacking sequences. For silver clusters in the range from Ag_{61} to Ag_{120},[25] as predicted from the Gupta potential, most clusters have decahedral motifs, except for nine non-decahedral patterns. Ag_{38} is a truncated octahedron, and Ag_{55} is an icosahedron, as predicted by GA and DFT calculations[18,26] and confirmed by electron diffraction measurements.[27]

Size-dependent properties of clusters have been studied for other metal clusters, such as Ni,[22] Cu,[22] Pb,[28] Cd,[29,30] and Zn.[29,30] However, among bimetallic clusters, most studies have been limited to relatively small clusters using Gupta potentials. Examples are the structural properties of bimetallic clusters with up to about 55 atoms, including Pt−Pd,[34] Cu−Au,[35,36] and Ni−Al.[37]

In this paper, we have concentrated on the main characteristics of Ag−Au nanoalloys of 1:1 composition, because these have high entropy of mixing in the bulk solid solution Ag−Au alloy. We attempt to identify size-dependent structural patterns up to 150 atoms, and we search for new magic numbers and novel types of chemical ordering. To achieve this, we have performed global optimization using a GA approach combined with DFT relaxation. Finally, we have considered the roles of composition and temperature in the size evolution of the equilibrium structures of Ag−Au nanoalloys.

RESULTS AND DISCUSSION

Energetic Stability. The energies, point groups, and atomic ordering for the putative global minima are given in Table 2. These clusters have low symmetries, and all have C_1 point group symmetry, except for $Ag_{10}Au_{10}$ (C_s), as predicted from the Gupta potential.

TABLE 2. Energies and Structures of Putative Global Minima for Ag−Au Nanoalloys Using the Gupta Potential[a]

N	*m*	$V_{cluster}$/eV	motif	*N*	*m*	$V_{cluster}$/eV	motif
20	0	−59.8055	twinned Ih_{13}	86	6	−272.3030	twinned Dh
22	0	−66.0641	twinned Ih_{13}	88*	4	−279.1388	twinned Dh
24*	0	−72.4511	twinned Ih_{13}	90	5	−285.5936	twinned Ih_{55}
26	0	−78.7359	twinned Ih_{13}	92	8	−292.0234	Dh
28	0	−85.1242	twinned Ih_{13}	94	8	−298.8105	Dh
30	0	−91.4427	twinned Ih_{13}	96	5	−305.3793	Dh
32	0	−97.8645	twinned Ih_{13}	98	9	−312.1650	Dh
34	0	−104.2488	twinned Ih_{13}	100	11	−318.7294	Dh
36	0	−110.6621	twinned Ih_{13}	102	10	−325.4572	Dh
38*	0	−117.3134	TO	104	11	−332.0059	Dh
40	0	−123.5324	Ih_{55}	106	10	−338.4055	Dh
42	1	−129.9734	twinned Ih_{13}	108	13	−344.7734	Dh
44	1	−136.2704	Ih_{55}	110	13	−350.8754	Dh
46	0	−142.8379	Ih_{55}	112	10	−357.9011	Dh
48	1	−149.3340	Ih_{55}	114	8	−364.4511	Dh
50	1	−155.7478	twinned Dh	116	10	−371.1731	Dh
52	1	−162.3814	Ih_{55}	118	12	−377.6619	Dh
54*	1	−169.0588	Ih_{55}	120	13	−383.5984	Dh
56	1	−175.4571	Ih_{55}	122	12	−390.2558	Dh
58	1	−181.8340	Ih_{55}	124*	17	−397.2184	Dh
60	2	−188.1643	Dh	126	13	−403.5111	Dh
62	1	−194.7674	twinned Ih_{55}	128	13	−409.6836	Dh
64	1	−201.1421	twinned Ih_{55}	130	14	−416.5153	Ih_{147}
66	2	−207.7146	twinned Ih_{55}	132	16	−423.0916	Ih_{147}
68	5	−214.0908	Dh	134	13	−429.7950	Ih_{147}
70	5	−220.7654	Dh	136	19	−436.5843	Ih_{147}
72	5	−227.1792	Dh	138	23	−442.8975	TO
74	4	−233.8269	Dh	140*	15	−450.2608	Ih_{147}
76*	2	−240.3646	Dh	142	12	−456.6665	Ih_{147}
78	8	−246.6945	Dh	144	18	−463.4801	Ih_{147}
80	6	−253.0306	Dh	146	19	−470.2259	Ih_{147}
82	5	−259.4811	twinned Dh	148	20	−476.6688	Ih_{147}
84	4	−265.7221	twinned Ih_{55}	150	22	−482.3981	Ih_{147}

[a]The symmetries of the clusters are C_1, except for $Au_{10}Ag_{10}$ ($N = 20$), which has C_s symmetry. *N* is the total number of atoms, *N** is a magic number (24, 38, 54, 76, 88, 124, 140), and *m* is the number of Ag atoms in core sites. Dh = capped decahedral clusters. Ih = defective or capped 13-, 55-, or 147-atom icosahedral clusters. TO = truncated octahedral clusters.

Ag_nAu_n clusters with $n = 10$–75 have no apparent overall order and may be described as disordered or amorphous, according to a formal definition of disorder as the absence of point group symmetry.

The energies of the global minima are represented in Figure 1 as a size-dependent stability function of Δ and Δ_2 in order to make particularly stable clusters stand out. Δ is the excess energy with respect to *N* bulk atoms, divided by $N^{2/3}$:

$$\Delta = \frac{E_{GM}^{N,N_1} - N_1\epsilon_1^{coh} - N_2\epsilon_2^{coh}}{N^{2/3}} \quad (1)$$

where E_{GM}^{N,N_1} is the global-minimum energy at the given size, ϵ_1^{coh} and ϵ_2^{coh} are the bulk cohesive energies of Ag and Au, and $N = 2N_1 = 2N_2$, where N_1 and N_2 are the numbers of Ag and Au atoms. Locally stable structures are identified as local minima in the plot of Δ vs *N*.

Δ_2 is the second difference in the energy:

$$\Delta_2^n = E_{GM}^{n+1} + E_{GM}^{n-1} - 2E_{GM}^n \quad (2)$$

Maxima in Δ_2 indicate structures of relative stability compared to those of nearby sizes (where $n = N/2$).

The energetic stability functions Δ and Δ_2 of clusters with different size are compared in Figure 1. The magnitude of the fluctuations arises from the differences between the more and less stable sizes. The local fluctuations in the second difference of the binding energies, Δ_2, are generally greater than those in the energetic stability function, Δ.

The function Δ does not show a smooth size dependence, as expected from the fully disordered clusters. Minima in Δ and maxima in Δ_2 both agree to single out the most stable cluster sizes, which are $N = 24$, 38, 54, 88, 124, and 140. The fcc 38-atom truncated octahedron is still a magic number cluster ($Ag_{19}Au_{19}$), and the magic numbers at $N = 54$ and 140 are associated with the 55- and 147-atom Mackay icosahedra after losing one or more vertex atoms because even-numbered clusters do not have complete icosahedral shells.

Chemical Ordering. The atomic or chemical ordering of the global minima is represented in Figure 2 as a size-dependent function of the number of Ag atoms in the core sites of the cluster. Previous studies[43] have found that alloy clusters of silver have polyicosahedal core–shell structures. Similar clusters are found in this work for $N = 20$–40 (also shown in Table 2): the cores of these clusters are composed completely of Au atoms, and all Ag atoms segregate at the surface; from $N = 42$ to 66 (except for $N = 60$), a single Ag atom occupies the core site while all other Ag atoms segregate to the surface, and there is a roughly even distribution of silver atoms on the surface, which reduces the surface energy.[3]

However, from $N = 68$ to $N = 150$, such core–shell chemical ordering, a surface-induced tendency toward non-bulk-like crystalline structures, is not necessary for the stability of larger Ag−Au clusters. The size-dependent mixing tendency in Ag−Au nanoalloys above 68 atoms is similar to that of the bulk Ag−Au alloy, an fcc-disordered solid solution, and at size $N =$ 138, the nanoalloy and bulk motifs have the same number of non-surface Ag atoms.

Geometries of Ag−Au Nanoalloys. The observed structures are depicted in Figures 3 and 4 for a selection of clusters that either are particularly stable or have some interesting structure feature. All clusters are described in Table 2.

The lowest-energy structure of the 24-atom cluster is an aggregate of three interpenetrating and face-sharing 13-atom icosahedra. As the cluster size increases from 20 to 36 atoms, chains and then planes of 13-atom icosahedra are seen. Icosahedral structures are inherently strained, as the distance between adjacent atoms on the surface of the regular 13-atom icosahedron is 5% longer than that to the central atom. The strain and the resulting energy cost grow rapidly with size, so that twinned 13-atom icosahedra evolve into bulk crystalline order at $N = 38$ and 2-shell icosahedra at $N = 40$–58 (with the exception of $N = 42$ and 50). These clusters are based on the 55-atom Mackay icosahedron, containing some vacancies for $N < 55$ or capping atoms for $N > 55$. As N increases from 60 to 66, structures go through a 60-atom decahedral intermediate (metastable isomer size) and fused 55-atom icosahedra; *e.g.*, the 62-atom cluster is a double 55-atom icosahedron with one twin plane. Therefore, the first icosahedral window is identified in the size range of 20–66 atoms for 1:1 Ag−Au nanoalloys, where structure is dominated by the local or global order of icosahedral symmetry and core–shell chemical order.

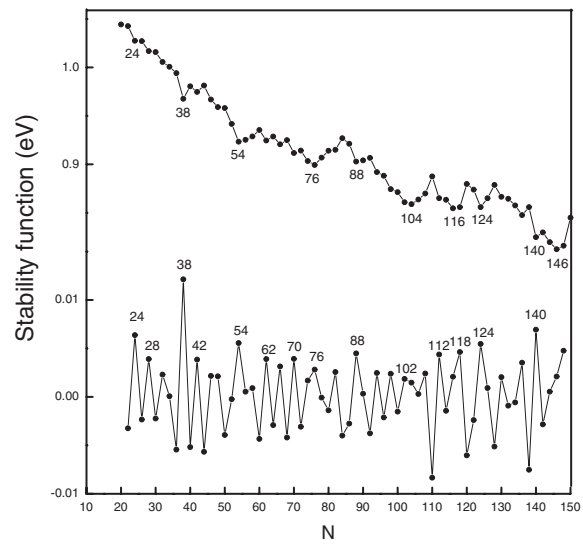

Figure 1. Energetic stability functions Δ (top) and Δ_2 (bottom) as a function of size ($N = 2n$) for $(AgAu)_n$ nanoalloys.

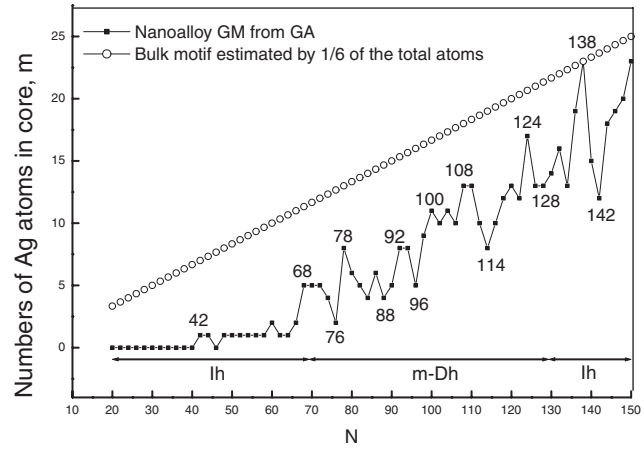

Figure 2. Number of Ag atoms in the core of clusters as a function of size ($N = 2n$) for $(AgAu)_n$ nanoalloys. Ih is an icosahedral window, and m-Dh is Marks decahedral window.

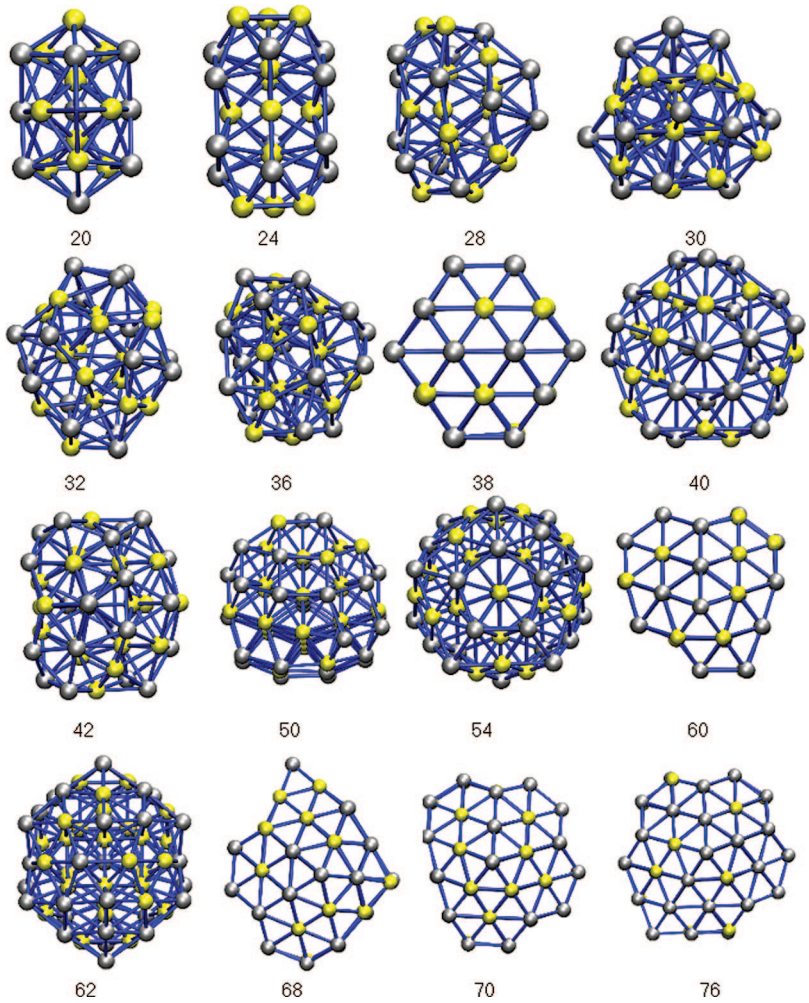

Figure 3. Typical geometries of $(AgAu)_n$ nanoalloys with 20–76 atoms. Gold atoms are shown in yellow.

The distorted Marks decahedral structure becomes energetically more favorable in the range $N = 68-128$. There are three magic number clusters at $N = 76$, 88, and 124 and two icosahedra at $N = 84$ and 90. Classical decahedra are constructed on pentagonal bipyramids,[29] while more stable Marks decahedra are produced[44,45] by five re-entrant facets introduced at the twin boundaries of the decahedron. The 98-atom cluster in Figure 4 is an example of incomplete Marks decahedra with five vertical grooves. The 76-atom magic cluster is associated with the 75-atom Marks decahedron with one capping atom on a groove. The 124-atom magic cluster is derived from the 122-atom Marks decahedron with two capping atoms on a groove. Such groove-bridged Marks decahedra have been identified as being particularly stable for cadmium[29] and gold[46] clusters.

The magic cluster at $N = 88$ is a new finding for bimetallic clusters in this study. A groove-bridged Marks decahedral structure is clearly discernible on its bottom part and two face-sharing decahedral fragments on its top. The 88-atom cluster, $Ag_{44}Au_{44}$, is a triply twinned decahedron; *i.e.*, it contains three classical decahedral motifs. It is a structure with polynanocrystalline order with three five-fold symmetry axes. Such polydecahedral clusters have recently been identified by molecular dynamics (MD) freezing simulations for pure gold clusters of 2–4 nm size.[47] From $N = 68$ to 126, there is a decahedral window, though there is also some tendency toward bulk-like crystalline structures and chemical order.

Beyond $N = 128$, the structures are dominated again by icosahedral structures; *i.e.*, there is another Ih window. There is one magic size cluster at $N = 140$ and one new fcc truncated octahedron at $N = 138$. The 140-atom magic cluster is a defective 147-atom Mackay icosahedron.

In summary, among the Ag_nAu_n clusters with 20−150 atoms, 31 decahedral clusters, 35 icosahedral clusters, and 2 close-packed motifs have been identified, distributed within two Ih windows and one m-Dh window.

Electronic Properties. Although we are confident with the series of candidate structures predicted from the Gupta potential, nine different Ag−Au nanoalloys have been reoptimized using DFT, and their electronic structures have been calculated.

The nine Ag−Au nanoalloys (Table 3) include all five magic clusters located by global optimization with $N < 100$ atoms. The other four clusters are the 20-atom cluster (the smallest cluster in the series), the 98-atom incomplete Marks decahedron, and two medium-sized (70- and 76-atom) decahedra. As shown in Figure 5, after DFT reoptimization, all the clusters retain their structures except $Ag_{10}Au_{10}$, the structure of which changes from a double face-sharing icosahedron of C_s point group symmetry into a capped 13-atom icosahe-

TABLE 3. Energies and Electronic Structures from DFT−GGA Calculations [a]

N	m	E_b/eV	IP^V/eV	EA/eV	HOMO/eV	LUMO/eV	E_{gap}/eV
20	0	1.8645	5.5853	2.3168	−4.200	−3.655	0.545
24*	0	1.9024	5.7029	2.6862	−4.435	−4.086	0.349
38*	0	2.1027	4.9802	2.4221	−3.727	−3.691	0.036
54*	1	2.1195	5.0549	2.7293	−3.979	−3.864	0.115
60	2	2.1333	5.0049	2.7633	−3.923	−3.697	0.226
70	5	2.1624	4.9620	2.8742	−3.938	−3.857	0.081
76*	2	2.1723	4.9334	2.9007	−4.014	−3.905	0.109
88*	4	2.2086	5.0092	3.0379	−4.030	−3.765	0.265
98	9	2.2268	4.8643	2.9848	−3.937	−3.855	0.082

[a] The symmetry of the $Au_{10}Ag_{10}$ ($N = 20$) cluster changes from C_s to C_1 after DFT reoptimization. E_b is the binding energy per atom, IP^V is the vertical ionization potential, EA is the electron affinity, HOMO and LUMO represent the highest occupied and lowest unoccupied molecular orbit energies, and E_{gap} is the HOMO−LUMO gap.

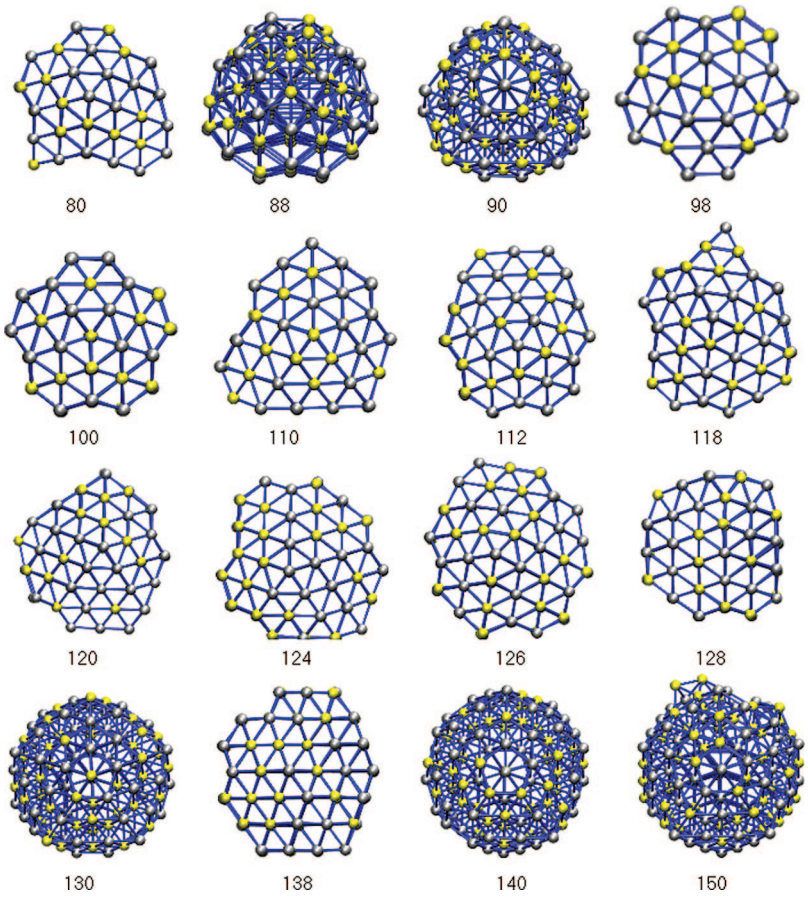

Figure 4. Typical geometries of $(AgAu)_n$ nanoalloys with 80–150 atoms. Gold atoms are shown in yellow.

dron with C_1 symmetry. The structure is characterized by a single Au atom core and a mixed Ag−Au shell. Bonacic-Koutecky *et al.*[48] predicted by DFT that $Ag_{10}Au_{10}$ adopts compact 3D structures characterized by a large number of Ag−Au bonds, and its geometry is the same double icosahedron as predicted by the Gupta potential in this study.

Surface reconstruction has been observed for the central Au atoms on the (111) facets on the 38-atom truncated octahedron and for Au atoms on re-entrant facets of Marks decahedra, as in the 98-atom cluster. The surface reconstruction corresponds to the outer Au atoms moving out of the crystalline plane or atomic column to the surface (Figure 5). The 54-atom icosahedron retains its structure after DFT reoptimization. It is interesting to note that the energy of groove-bridged Marks decahedra can be further improved by this surface reconstruction, which is consistent with the tendency for Au atoms to occupy the outer sites of small Ag−Au clusters.[48,49] The Au atom rearrangement (upward to the surface) apparently derives from the anisotropic or bond directionality, as previously observed in a pure Pt cluster.[50] Gold, in fact, is a third-row metal, in which the relativistic contraction of the s orbital brings it to overlap with the d orbitals, decreasing the localized character of the latter and strongly increasing their contribution to chemical bonding.

The electronic properties of the DFT-reoptimized structures are listed in Table 3 and depicted in Figure 6. The average binding energy per atom, E_b, the energy necessary to atomize the cluster completely, increases with the number of atoms as expected. The ionization potentials and electron affinities converge to the intrinsic work function of the bulk alloys as the number of atoms increases. The HOMO−LUMO gap decreases as cluster size increases. At the bulk limit, the gap is zero as the HOMO and LUMO both converge to the Fermi level of the alloy. The gap exhibits some fluctuations, as for pure gold clusters,[21] and two peaks are obtained at $N = 60$ and 88. It is worth noting that

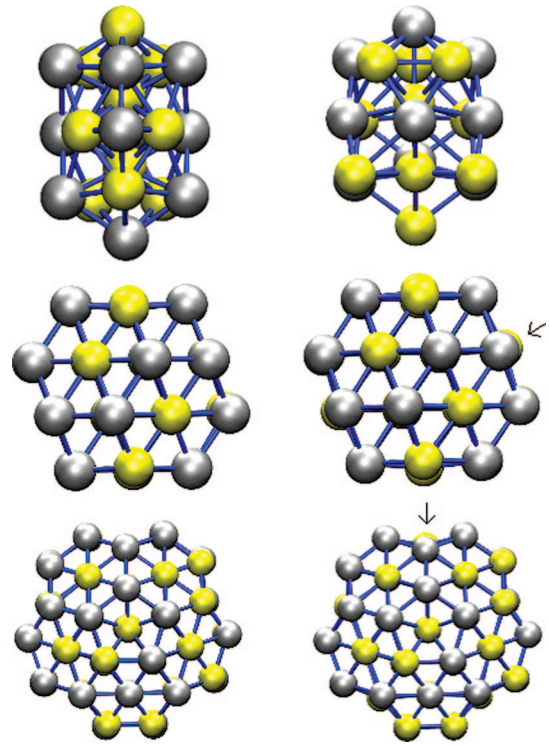

Figure 5. Geometries of $(AgAu)_n$ nanoalloys with 20 (first row), 38 (second row), and 98 (third row) atoms before (left) and after (right) DFT reoptimization. The arrow points to the reconstructed Au atoms underneath.

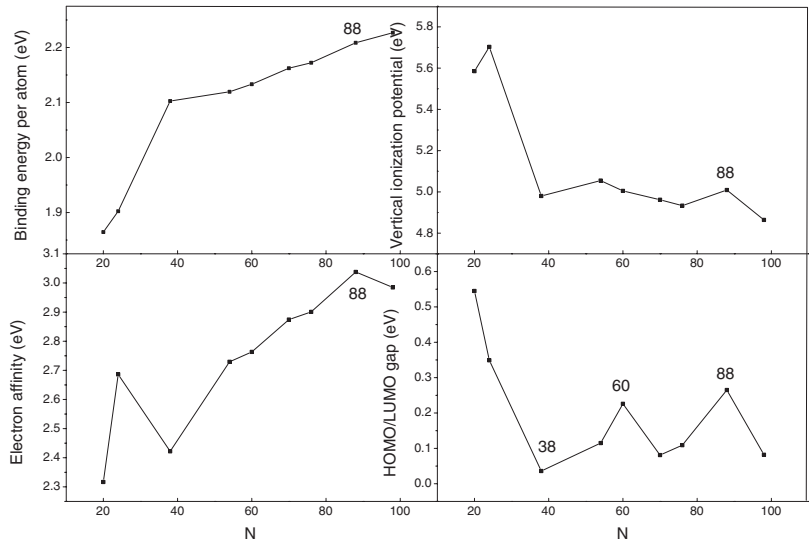

Figure 6. DFT-calculated electronic properties for $(AgAu)_n$ nanoalloys as a function of size ($N = 2n$).

the 88-atom cluster yields a larger gap (0.265 eV) and higher one-electron energy than the neighboring clusters.

The binding energies calculated at the DFT level, as shown in Table 3, are 1.8645 and 2.2268 eV/atom for $N = 20$ and 98, respectively, while the Gupta potential binding energies for the same clusters, as calculated from the total cluster potential energies in Table 2, using eq 4 (shown in the Methodology section), are 2.9903 and 3.1854 eV/atom, respectively. Recent work on Ag[51] and Pd−Pt[52] clusters indicate that the outcome of simulations varies with the potential energy function. The Gupta potential used here has been fitted to experimental properties of the bulk metals and alloys and is expected to be less accurate than the DFT-based energy model for small sizes, especially below 20 atoms. The main drawback of this empirical potential is the lack of specific quantum effects, such as shell-closure, electronic wave function interference, and directionality effects. However, it is important to note that the many-body character of this empirical potential provides a reasonably accurate model for metallic systems and enables thorough exploration of the potential energy surface using global optimization methods.

Melting Behavior. The thermal effect or finite-temperature behavior of the metal cluster has attracted much attention since the previous experimental work[53,54] and atomic simulations[55,56] on sodium clusters and gold clusters.[57] The melting behavior of nanoclusters is highly dependent on cluster size and lowest-energy structure and can be used to explore the structural properties.[58]

Figure 7 shows the caloric curves calculated for the 38- and 138-atom truncated octahedral Ag−Au nanoalloys. All fcc truncated octahedral clusters show a well-defined melting transition upon heating, *i.e.*, a jump or sharp change in the caloric curve, with the difference of total energy between the solid and liquid phases being the latent heat of melting.

The caloric curves of the decahedral clusters with 60, 70, 76, 88, 98, 112, 118, and 124 atoms are shown in Figure 8. The 60-atom cluster shows a gradual evolution of the solid cluster toward the liquid state due to melting from the surface inward.[59] There is a general increase in melting temperature with increasing size, except for the anomalously high values for $N = 76$ and 118, which is an example of finite size effects, as observed in many small clusters such as Ni clusters.[60]

Figure 9 shows the caloric curves of 24-, 28-, 32-, 36-, 42-, 54-, 62-, and 140-atom Ag−Au icosahedral nanoalloys. The 24-, 28-, and 62-atom clusters show a gradual melting transition, while all the others show a sharp melting transition. The 36-atom cluster melts at a higher temperature than the 42-atom cluster, as do the 54- and 62-atom clusters. The 54-atom cluster shows an oscillation in the caloric curve, possibly due to permutational isomers which compete with liquid-like isomers, leading to pre-melting of the cluster.

Figures 7−9 show that none of the clusters relax into a lower-energy state (manifested as a drop in the caloric curve) when heating from 0 K to the melting point. This indicates that the starting structures are probably global minima or are very close in energy and structure to the global minimum. In contrast to our previous findings for 55-atom pure Au and Au-rich Ag−Au nanoalloys,[58] no glass-like transition is observed for any of the clusters. This indicates that the structures of the clusters are distinct from the liquid metal and have some medium-range or global crystalline order. None of the clusters have disordered global minima, which is in contrast to pure Au clusters (even for some magic number sizes[17,18]), which exhibit many intermediate-size dis-

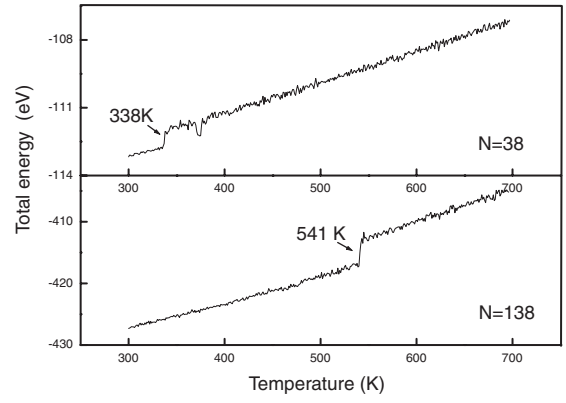

Figure 7. Caloric curves for truncated octahedral $(AgAu)_n$ nanoalloys with 38 and 138 atoms from 300 to 700 K.

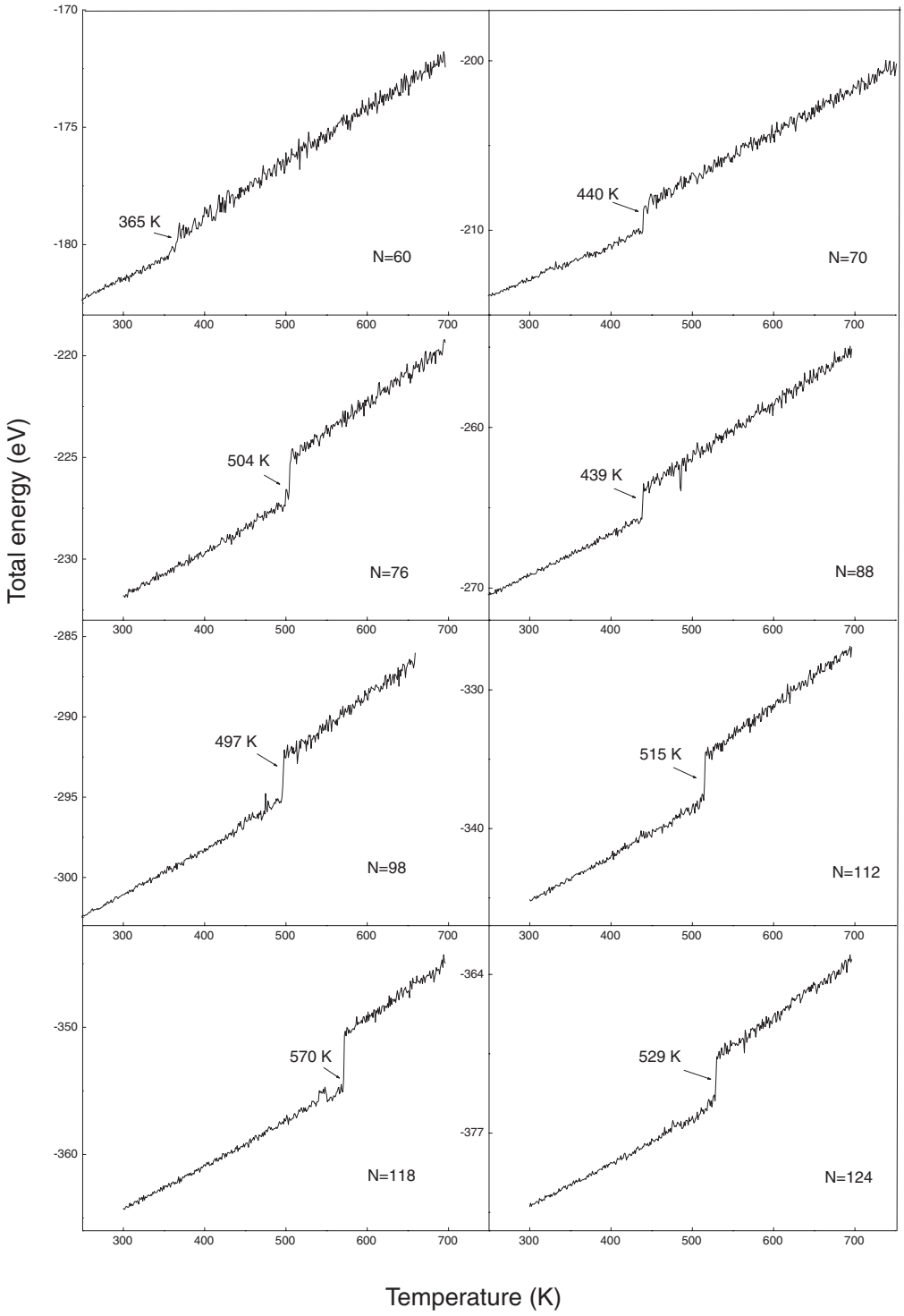

Figure 8. Caloric curves of decahedral $(AgAu)_n$ nanoalloys with 60, 70, 76, 88, 98, 112, 118, and 124 atoms from 300 to 700 K.

ordered global minima,[19] and pure Ag clusters, whigh have many small disordered global minima,[61] as predicted from the same Gupta potential. Thus, for the 1:1 composition, it appears that alloying leads to the stabilization of geometrically ordered structures.

It is important to note that, in nanoalloys, the local structure present in the disordered clusters could be assembled in a way that gives rise to a particularly stable cluster with new structural motifs. Examples have previously been found in bulk alloys[62,63] and recently in metallic glasses,[64,65] where truncated tetrahedral local order can be stabilized through just two types of atoms to form bulk polytetrahedral crystals, the Frank−Kasper phases.[62] In these disordered Ag−Au nanoalloys, particularly

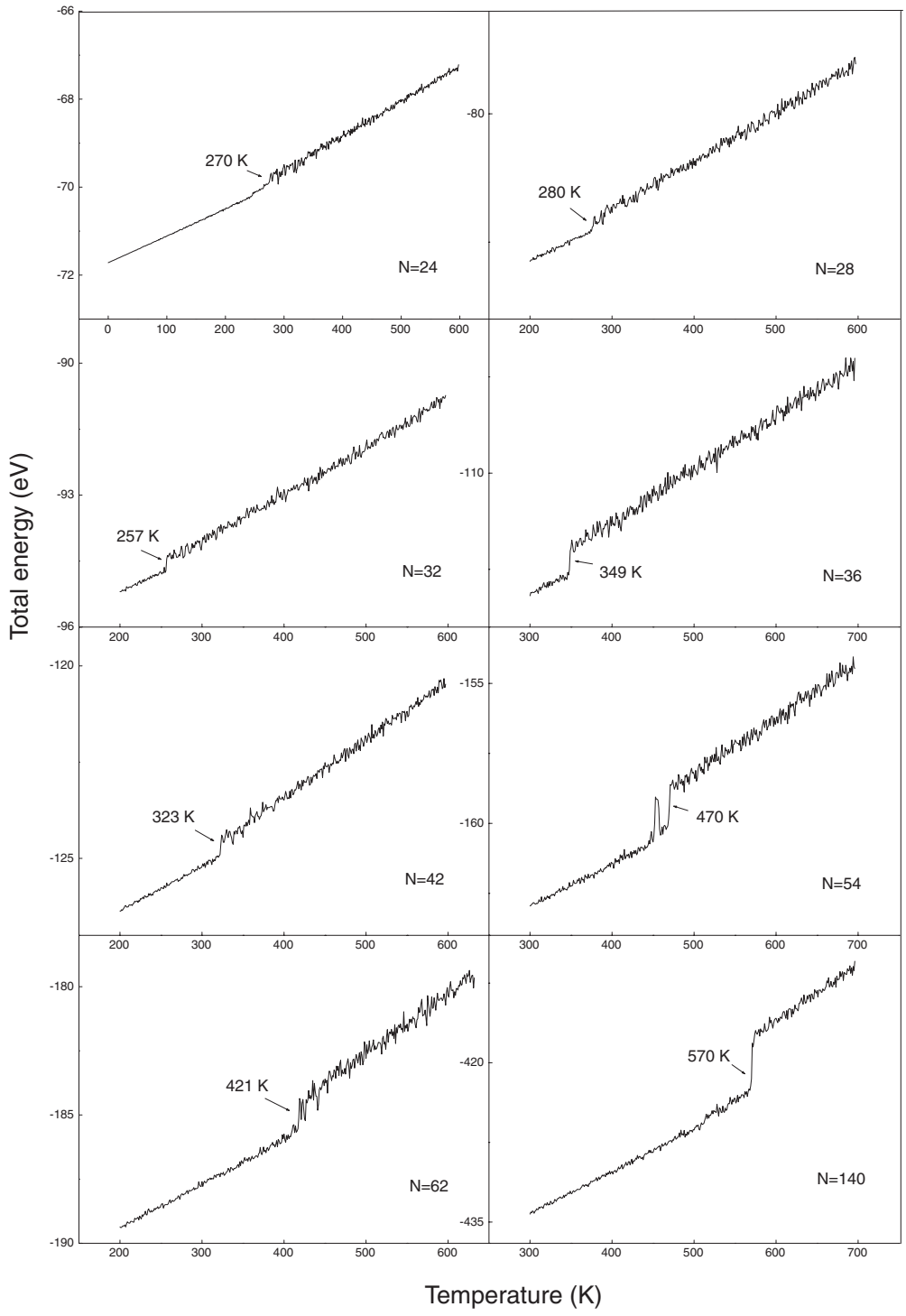

Figure 9. Caloric curves of icosahedral $(AgAu)_n$ nanoalloys with 24, 28, 32, 36, 42, 54, 62 and 140 atoms up to 700 K.

stable clusters with new motifs have been realized, for example, the 24-atom twinned Ih_{13} cluster and the 88-atom twinned Dh cluster.

CONCLUSIONS

The complexity of the structural behavior of Ag−Au nanoalloys derives from the combination of the core–shell chemical ordering of Ag alloy clusters and the amorphous crystalline habits of Au alloy clusters.

In this study, the lowest-energy structures of 1:1 Ag−Au nanoalloys containing 20−150 atoms have been searched using a global optimization approach. These clusters have low-symmetry C_1 point group structures with twinned, capped, defective, and distorted atomic packing. In all, 31 decahedra,

35 icosahedra, and 2 close-packed motifs have been identified. Magic numbers have been observed for $N = 24$, 38, 54, 76, 88, 124, and 140. A set of icosahedron-dominated structural motifs, the "Ih window", is obtained in the size range 20–66, changing to a Marks-Dh window in the size range 68–128, and then another Ih window in the size range 130–150. The size-dependent structural transition in Ag−Au nanoalloys is so strongly related to the magic icosahedral numbers 55 and 147 that we can predict that the next Ih window will appear around the magic numbers 309 and 561, and between them, there should be a new Marks-Dh window.

Other properties of Ag−Au nanoalloys converge to the bulk alloy very rapidly instead of varying periodically with size. Chemical (atomic) ordering changes from core–shell to bulk-like mixed solid solution disorder from 68 atoms. Electronic structure calculations using density functional theory reproduce the geometries predicted by the GA for clusters larger than 24 atoms. The electronic effects tend to rearrange the Au atoms onto the surface of the structures predicted by the Gupta potential. The melting behavior studies show that the entire clusters exhibit a bulk-like first-order melting transition, though for some sizes the transition is sharp and for others it is gradual. A new polynanocrystalline decahedral motif, $Ag_{44}Au_{44}$, is found to have high structural, electronic, and thermal stability.

After the submission of this manuscript, recent experimental work[42] was reported on the structure and crystallization of Au_{102} cluster passivated by 44 thiolate ligands. The cluster has a decahedral structure, with a 49-atom Marks-Dh core and is characterized by a 58-electron closed electronic shell. The topology is consistent with the present work, in that our predicted structure for $(AgAu)_{51}$ is based on a Marks-Dh, though the ligands in the experimental structure give rise to a reconstruction of the surface atoms."

METHODOLOGY

The energetic model used in the global optimizations and MD simulations reported here is the many-body Gupta potential,[66] which is derived from the second-moment approximation to tight binding theory, extended to the description of alloys. Its analytical form is as follows:

$$V_{\text{cluster}} = \sum_{i}^{N}\left(\sum_{i\neq j}^{N} A\, e^{-p\bar{r}_{ij}} - \sqrt{\sum_{i\neq j}^{N} \xi^2\, e^{-2q\bar{r}_{ij}}}\right) \quad (3)$$

where N is the number of atoms, $\bar{r}_{ij} = r_{ij}/r_0 - 1$, and $r_{ij} = |r_i - r_j|$ is the distance between atoms i and j. The Gupta potential parameters for Ag−Au nanoalloys are listed in Table 1.

Global optimization was performed using the Birmingham cluster genetic algorithm (BCGA).[67] The genetic algorithm is a population-based search technique to find the optimum solution in a multidimensional parameter space. It is based on principles of natural evolution, using operators which have analogues in the theory of biological evolution, such as mating, mutation, and natural selection. It explores many different solutions simultaneously. and each investigation reveals information about a different region of the surface. BCGA acts on the phenotype (*i.e.*, the 3D cluster structure) rather than the genotype (encoded coordinates).[9,10] In this work, the following genetic algorithm parameters were employed: population size = 38, mating rate = 0.8, crossover type = one-point, mutation rate = 0.1, and number of generations = 500.

During the geometry optimization, 20 GA runs (with different random number seeds) were carried out for each composition, and the resultant structures were then analyzed by comparing the average binding energy, E_b, for an N-atom cluster, which is defined as

$$E_b = \frac{-V_{\text{cluster}}}{N} \quad (4)$$

where V_{cluster} is the total cluster potential energy.

DFT calculations[68] were then carried out on selected configurations. The spin-polarized DFT calculations were performed in real space within the framework of the DFT-based relativistic semicore pseudopotential[69] with double numerical basis sets with d-polarization functions. A global cutoff of 4.5 Å was used for grid integration. Self-consistent field procedures were performed with a convergence criterion of 10^{-6} au on the total energy and electron density. The generalized gradient approximation (GGA) functional of Perdew, Burke, and Ernzerhof[70] was used for exchange-correlation during the geometry and property calculations.

MD simulations[71] were used to study the melting of Ag−Au nanoalloys. Newton's equations were solved using the velocity Verlet algorithm,[72] with a time step of 7 fs. The temperature was controlled by an Andersen thermostat and was increased by scaling up the velocities in a step-like manner, each step corresponding to an increase of 1 K. The heating rate was 0.8–4 K/ns; the accuracy of the current computational scheme was checked by making benchmark calculations on the icosahedral Ag_{55} cluster. The average melting point from our calculations is 565 K, which agrees well with previous simulation results (570 K)[73] using the same Gupta potential parameters. During individual simulation runs, the different melting pathways were directly observed by taking atomic configuration snapshots and plotting the caloric curves calculated by taking time averages of the total energy as a function of thermostat temperature, $E(T)$.

Acknowledgment. F.Y.C. acknowledges financial support from the Natural Science Foundation of China (No. 50671082) and Shaanxi Province (No. 2006CS040002), and the Aeronautic Science Foundation (No. 05G530038) of China. The authors thank Dr. G. Rossi (University of Genoa) for helpful discussions and for preparing the figure for the table of contents.

Supporting Information Available: Complete structural data of the $Ag_{44}Au_{44}$ nanoalloy, as well as the RosMol script to show the three five-fold symmetry axes. This information is available free of charge *via* the Internet at http://pubs.acs.org.

REFERENCES AND NOTES

1. Johnston, R. L. *Atomic and Molecular Clusters*; Taylor and Francis: London, 2002.
2. Wales, D. J.; Scheraga, H. A. Global Optimization of Clusters, Crystals, and Biomolecules. *Science* **1999**, *285*, 1368–1372.
3. Ferrando, R.; Jellinek, J.; Johnston, R. L. Nanoalloys: From Theory to Applications of Alloy Clusters and Nanoparticles. *Chem. Rev.*, in press.

4. Lee, K.-S.; El-Sayed, M. A. Gold and Silver Nanoparticles in Sensing and Imaging: Sensitivity of Plasmon Response to Size, Shape, and Metal Composition. *J. Phys. Chem. B* **2006**, *110*, 19220–19225.
5. Benten, W.; Nilius, N.; Ernst, N.; Freund, H. J. Photon Emission Spectroscopy of Single Oxide-supported Ag−Au Alloy Clusters. *Phys. Rev. B* **2005**, *72*, 045403.
6. Bruzzone, S.; Malvavaldi, M.; Arrighini, G. P.; Guidotti, C. Near-Field and Far-Field Scattering by Bimetallic Nanoshell Systems. *J. Phys. Chem. B* **2006**, *110*, 11050–11054.
7. Krissinel, E. B.; Jellinek, J. 13-atom Ni-Al Alloy Clusters: Correlation between Structural and Dynamical Properties. *Chem. Phys. Lett.* **1997**, *272*, 301–312.
8. Doye, J. P. K.; Wales, D. J. Polytetrahedral Clusters. *Phys. Rev. Lett.* **2001**, *86*, 5719–5722.
9. Deaven, D. M.; Ho, K. M. Molecular-Geometry Optimization with a Genetic Algorithm. *Phys. Rev. Lett.* **1995**, *75*, 288–291.
10. Deaven, D. M.; Tit, N.; Morris, J.; R.; Ho, K. M. Structural Optimization of Lennard-Jones Clusters by a Genetic Algorithm. *Chem. Phys. Lett.* **1996**, *256*, 195–200.
11. Wales, D. J.; Doye, J. P. K. Global Optimization by Basin-Hopping and the Lowest Energy Structures of Lennard-Jones Clusters Containing up to 110 Atoms. *J. Phys. Chem. A* **1997**, *101*, 5111–5116.
12. Doye, J. P. K. Effect of Compression on the Global Optimization of Atomic Clusters. *Phys. Rev. E* **2000**, *62*, 8753–8761.
13. Barron, C.; Gomez, S.; Romero, D.; Saavedra, A. A. Genetic Algorithm for Lennard-Jones Atomic Clusters. *Appl. Math. Lett.* **1999**, *12*, 85–90.
14. Pullan, W. J. Genetic Operators for the Atomic Cluster Problem. *Comput. Phys. Commun.* **1997**, *107*, 137–148.
15. Leary, R. H.; Doye, J. P. K. Tetrahedral Global Minimum for the 98-atom Lennard-Jones Cluster. *Phys. Rev. E* **1999**, *60*, R6320–R6322.
16. Doye, J. P. K.; Wales, D. J.; Miller, M. A. Thermodynamics and the Global Optimization of Lennard-Jones Clusters. *J. Chem. Phys.* **1998**, *109*, 8143–8153.
17. Garzon, I. L.; Michaelian, K.; Beltran, M. R.; Posada-Amarillas, A.; Ordejon, P.; Artacho, E.; Sanchez-Portal, D.; Soler, J. M. Lowest Energy Structures of Gold Nanoclusters. *Phys. Rev. Lett.* **1998**, *81*, 1600–1603.
18. Michaelian, K.; Rendon, N.; Garzon, I. L. Structure and Energetics of Ni, Ag, and Au Nanoclusters. *Phys. Rev. B* **1999**, *60*, 2000–2010.
19. Soler, J. M.; Beltran, M. R.; Michaelian, K.; Garzon, I. L.; Ordejon, P.; Sanchez-Portal, D.; Artacho, E. Metallic Bonding and Cluster Structure. *Phys. Rev. B* **2000**, *61*, 5771–5780.
20. Sutton, A. P.; Chen, J. Long-Range Finnis Sinclair Potentials. *Philos. Mag. Lett.* **1990**, *61*, 139–146.
21. Haberlen, O. D.; Chung, S. C.; Stener, M.; Rosch, N. From Clusters to Bulk: A Relativistic Density Functional Investigation on a Series of Gold Clusters Au_n, n=6, 147. *J. Chem. Phys.* **1997**, *106*, 5189–5201.
22. Doye, J. P. K.; Wales, D. J. Global Minima for Transition Metal Clusters Described by Sutton-Chen Potentials. *New J. Chem.* **1998**, *22*, 733–744.
23. Cleveland, C. L.; Landman, U.; Schaaff, T. G.; Shafigullin, M. N.; Stephens, P. W.; Whetten, R. L. Structural Evolution of Smaller Gold Nanocrystals: The Truncated Decahedral Motif. *Phys. Rev. Lett.* **1997**, *79*, 1873–1876.
24. Alamanova, D.; Grigoryan, V. G.; Springborg, M. Theoretical Study of Structure and Energetics of Gold Clusters with the EAM Method. *Z. Phys. Chem.* **2006**, *220*, 811–829.
25. Zhan, H.; Cheng, L. J.; Cai, W. S.; Shao, X. G. Structural Optimization of Silver Clusters from Ag_{61} to Ag_{120} by Dynamic Lattice Searching Method. *Chem. Phys. Lett.* **2006**, *422*, 358–362.
26. Baletto, F.; Rapallo, A.; Rossi, G.; Ferrando, R. Dynamical Effects in the Formation of Magic Cluster Structures. *Phys. Rev. B* **2004**, *69*, 235421.
27. Xing, X. P.; Danell, R. M.; Garzon, I. L.; Michaelian, K.; Blom, M. N.; Burns, M. M.; Parks, J. H. Size-Dependent Fivefold and Icosahedral Symmetry in Silver Clusters. *Phys. Rev. B* **2005**, *72*, 081405.
28. Doye, J. P. K. Lead clusters: Different potentials, Different structures. *Comput. Mater. Sci.* **2006**, *35*, 227–231.
29. Doye, J. P. K. Identifying Structural Patterns in Disordered Metal Clusters. *Phys. Rev. B* **2003**, *68*, 195418.
30. Michaelian, K.; Beltran, M. R.; Garzon, I. L. Disordered Global-minima Structures for Zn and Cd Nanoclusters. *Phys. Rev. B* **2002**, *65*, 041403.
31. Doye, J. P. K.; Wales, D. J.; Branz, W.; Calvo, F. Modeling the Structure of Clusters of C-60 Molecules. *Phys. Rev. B* **2001**, *64*, 235409.
32. Ho, K. M.; Shvartsburg, A. A.; Pan, B. C.; Lu, Z. Y.; Wang, C. Z.; Wacker, J. G.; Fye, J. L.; Jarrold, M. F. Structures of Medium-sized Silicon Clusters. *Nature* **1998**, *392*, 582–585.
33. Chan, T. L.; Ciobanu, C. V.; Chuang, F. C.; Lu, N.; Wang, C. Z.; Ho, K. M. Magic Structures of H-Passivated 110 Silicon Nanowires. *Nano Lett.* **2006**, *6*, 277–281.
34. Massen, C.; Mortimer-Jones, T. V.; Johnston, R. L. Geometries and Segregation Properties of Platinum-Palladium Nanoalloy Clusters. *J. Chem. Soc., Dalton Trans.* **2002**, *23*, 4375–4388.
35. Darby, S.; Mortimer-Jones, T. V.; Johnston, R. L.; Roberts, C. Theoretical Study of Cu-Au Nanoalloy Clusters Using a Genetic Algorithm. *J. Chem. Phys.* **2002**, *116*, 1536–1550.
36. Lordeiro, R. A.; Guimaraes, F. F.; Belchior, J. C.; Johnston, R. L. Determination of Main Structural Compositions of Nanoalloy Clusters of Cu_xAu_y ($x+y <= 30$) using a Genetic Algorithm Approach. *Int. J. Quantum Chem.* **2003**, *95*, 112–125.
37. Bailey, M. S.; Wilson, N. T.; Roberts, C.; Johnston, R. L. Structures, Stabilities and Ordering in Ni-Al Nanoalloy Clusters. *Eur. Phys. J. D* **2003**, *25*, 41–55.
38. Roberts, C.; Johnston, R. L. Investigation of the Structures of MgO Clusters using a Genetic Algorithm. *Phys. Chem. Chem. Phys.* **2001**, *3*, 5024–5034.
39. Costales, A.; Blanco, M. A.; Francisco, E.; Pendas, A. M.; Pandey, R. First Principles Study of Neutral and Anionic (Medium-Size) Aluminum Nitride Clusters: Al_nN_n, n = 7–16. *J. Phys. Chem. B* **2005**, *110*, 4092–4098.
40. Costales, A.; Kandalam, A. K.; Pandey, R. Theoretical Study of Neutral and Anionic Group III Nitride Clusters: M_nN_n (M = Al, Ga, and In; n = 4–6). *J. Phys. Chem. B* **2003**, *107*, 4508–4514.
41. Doye, J. P. K.; Meyer, L. Mapping the Magic Numbers in Binary Lennard-Jones Clusters. *Phys. Rev. Lett.* **2005**, *95*, 063401.
42. Jadzinsky, P. D.; Calero, G.; Ackerson, C. J.; Bushnell, D. A.; Kornberg, R. D. Structure of a Thiol Monolayer-Protected Gold Nanoparticles at 1.1 Å Resolutions. *Science* **2007**, *318*, 430–433.
43. Rossi, G.; Rapallo, A.; Mottet, C.; Fortunelli, A.; Baletto, F.; Ferrando, R. Magic Polyicosahedral Core-Shell Clusters. *Phys. Rev. Lett.* **2004**, *93*, 105503.
44. Marks, L. D.; Smith, D. J. Direct Surface Imaging in Small Metal Particles. *Nature* **1983**, *303*, 316–317.
45. Marks, L. D. Experimental Studies of Small-Particle Structures. *Rep. Prog. Phys.* **1994**, *57*, 603–649.
46. Soler, J. M.; Garzon, I. L.; Joannopoulos, J. D. Structural Patterns of Unsupported Gold Clusters. *Solid State Commun.* **2001**, *117*, 621–625.
47. Rossi, G.; Ferrando, R. Freezing of Gold Nanoclusters into Poly-decahedral Structures. *Nanotechnology* **2007**, *18*, 225706.
48. Bonacic-Koutecky, V.; Burda, J.; Mitric, R.; Ge, M. F.; Zampella, G.; Fantucci, P. Density Functional Study of Structural and Electronic Properties of Bimetallic Silver-gold Clusters: Comparison with Pure Gold and Silver clusters. *J. Chem. Phys.* **2002**, *117*, 3120–3131.
49. Chen, F. Y.; Johnston, R. L. Structure and Spectral Characteristics of the Nanoalloy Ag_3Au_{10}. *Appl. Phys. Lett.* **2007**, *90*, 153123.

50. Apra, E.; Baletto, F.; Ferrando, R.; Fortunelli, A. Amorphization Mechanism of Icosahedral Metal Nanoclusters. *Phys. Rev. Lett.* **2004**, *93*, 065502.
51. Yukna, J.; Wang, L. C. Molecular Dynamics Studies of the Coalescence of Silver Clusters. *J. Phys. Chem. C* **2007**, *111*, 13337–13347.
52. Paz-Borbon, L. O.; Johnston, R. L.; Barcaro, G.; Fortunelli, A. A Mixed Structural Motif in 34-atom Pd−Pt Clusters. *J. Phys. Chem. C* **2007**, *111*, 2936–2941.
53. Schmidt, M.; Kusche, R.; Kronmuller, W.; von Issendorff, B.; Haberland, H. Experimental Determination of the Melting Point and Heat Capacity for a Free Cluster of 139 Sodium Atoms. *Phys. Rev. Lett.* **1997**, *79*, 99–102.
54. Schmidt, M.; Kusche, R.; Hippler, T.; Donges, J.; Kronmuller, W.; von Issendorff, B.; Haberland, H. Negative Heat Capacity for a Cluster of 147 Sodium Atoms. *Phys. Rev. Lett.* **2001**, *86*, 1191–1194.
55. Calvo, F.; Spiegelmann, F. Geometric Size Effects in the Melting of Sodium Clusters. *Phys. Rev. Lett.* **1999**, *82*, 2270–2273.
56. Doye, J. P. K.; Calvo, F. Entropic Effects on the Size Dependence of Cluster Structure. *Phys. Rev. Lett.* **2001**, *86*, 3570–3573.
57. Cleveland, C. L.; Luedtke, W. D.; Landman, U. Melting of Gold Clusters: Icosahedral Precursors. *Phys. Rev. Lett.* **1998**, *81*, 2036–2039.
58. Chen, F. Y.; Curley, B. C.; Rossi, G.; Johnston, R. L. Structure, Melting, and Thermal Stability of 55 Atom Ag−Au Nanoalloys. *J. Phys. Chem. C* **2007**, *111*, 9157–9165.
59. Aguado, A.; Lopez, J. M. Small Sodium Clusters that Melt Gradually: Melting Mechanisms in Na_{30}. *Phys. Rev. B* **2006**, *74*, 115403.
60. Teng, Y. Y.; Zeng, X. H.; Zhang, H. Y.; Sun, D. Y. Melting and Glass Transition for Ni clusters. *J. Phys. Chem. B* **2007**, *111*, 2309–2312.
61. Yang, X. L.; Cai, W. S.; Shao, X. G. Structural Variation of Silver Clusters from Ag_{13} to Ag_{160}. *J. Phys. Chem. A* **2007**, *111*, 5048–5056.
62. Nelson, D. R. Polytetrahedral Order in Condensed Matter. *Solid State Phys.* **1989**, *42*, 1–90.
63. Spaepen, F.; Nelson, D. R. Order in Metallic Glasses and Icosahedral Crystals. *Phys. Rev. B* **1985**, 4592–4606.
64. Sheng, H. W.; Luo, W. K.; Alamgir, F. M.; Bai, J. M.; Ma, E. Atomic Packing and Short-to-medium-range Order in Metallic Glasses. *Nature* **2006**, *439*, 419–425.
65. Sheng, H. W.; Liu, H. Z.; Cheng, Y. Q.; Wen, J.; Lee, P. L.; Luo, W. K.; Shastri, S. D.; Ma, E. Polyamorphism in a Metallic Glass. *Nat. Mater.* **2007**, *6*, 192–197.
66. Gupta, R. P. Lattice-relaxation at a Metal-surface. *Phys. Rev. B* **1981**, *23*, 6265–6270.
67. Johnston, R. L. Evolving Better Nanoparticles: Genetic Algorithms for Optimising Cluster Geometries. *Dalton Trans.* **2003**, 4193–4207.
68. Delley, B. All-Electron Numerical-Method for Solving the Local Density Functional for Polyatomic-Molecules. *J. Chem. Phys.* **1990**, *92*, 508–517.
69. Hamann, D. R.; Schluter, M.; Chiang, C. Norm-Conserving Pseudopotentials. *Phys. Rev. Lett.* **1979**, *43*, 1494–1497.
70. Perdew, J. P.; Burke, K.; Ernzerhof, M. Generalized Gradient Approximation Made Simple. *Phys. Rev. Lett.* **1996**, *77*, 3865–3868.
71. The MD program was kindly provided by Prof. R. Ferrando, Dipartimento di Fisica dell'Università di Genova, via Dodecaneso 33, 16146 Genova, Italy.
72. Verlet, L. Computer Experiments on Classical Fluids I. Thermodynamical Properties of Lennard-Jones Molecules. *Phys. Rev.* **1967**, *159*, 98.
73. Mottet, C.; Rossi, G.; Baletto, F.; Ferrando, R. Single Impurity Effect on the Melting of Nanoclusters. *Phys. Rev. Lett.* **2005**, *95*, 035501.